

# Chapter 6

## Robust State-Feedback Control of Electric Spring: Linear Matrix Inequality Approach of Linear Quadratic Regulator Design

### 6.1 Introduction

A *PI* controller can not cater effectively to the dynamism considered in the system of *ES*, as it may not satisfactorily comply with the demand of larger bandwidth, robustness, higher gain, and phase margin. Further, the results of the Cascaded-*PI* controller showed a considerable improvement in the voltage regulating capabilities, as presented in Chapter:4 due to the control of one additional state of the system. The improved results have led us to think about implementing the state feedback control and having a check on each and every state of the system.

The literature on the control of *VSC* has witnessed methods employing  $H_2$ - $H_\infty$  [116],  $\mu$ -synthesis and many more modern control techniques, which happen to be better than a *PI* controller but arduous and quite involving as far as their design and implementation are concerned.

Surprisingly, Robust and optimal control have not been presented in any available literature on the *ES*. Robust control is one such area of control that considers non-linearity and parametric uncertainties of the model. The controller needs excellent robustness to

counter the impact of variations in the system's parameters and the variation in the grid's impedance, as presented in the Sec:2.6 of Chapter:2; while controlling the *ES*. Further, the DC bus voltage may vary due to variation in the load and the state of the battery's charge.

State-space model and hence state feedback control has been proven to be the more effective and comprehensive control strategy as that compared to the conventional or classical control system [117][118][119] which is being designed and implemented using only single variable feedback through transfer function approach. State feedback control alone cannot eliminate steady-state errors. An integrator is required in conjunction with state feedback to achieve zero steady-state error. Proper design of the closed-loop state feedback controller, possessing an integrator, can offer stability to the converter connected to a weak grid also. Classical control theory has provided the founding basis for the output feedback closed-loop control, wherein modern control has provided the impetus to the regime of complete state feedback control, by taking into account all the states of a given system as feedback.

Different control strategies such as deadbeat control, the classical controller being designed using pole placement technique [120], linear quadratic regulator (*LQR*) being designed using Ackerman's formula or by solving the algebraic Riccati equation, could be used for the controller design of a grid-connected inverter. Realizing the deadbeat control could be achieved by placing all the poles at the origin but is subjected to the variation in switching frequency, leading to complications in the filter design, and further its controller design. Method of pole placement using bode plot and Nyquist plot could be used. Further, the design of *PI* or proportional resonant (*PR*) controller has proven to be simple and straightforward, but the controller is so designed will be operating with non-optimal control effort.

This chapter's prime objective is to design a state feedback controller using the linear quadratic regulator. The state feedback controller's gain matrix is to be designed optimally by using the numerical convex optimization method of linear matrix inequalities (*LMIs*), with an assumption that all the system states are observable.

## 6.2 Precursors of the Optimal Control of Electric Spring using Linear Quadratic Regulator

The Linear Quadratic Regulator (*LQR*) [95] [121] is an approach of control that can provide robustness to the control, based on the selection of weighted cost functions of the states and the inputs. *LQR* can provide Phase Margin, ( $P.M.$ )  $> 70^\circ$  and more significant Gain Margin ( $G.M.$ ), which is much anticipated for efficient control and greater bandwidth, which further leads to robustness against parametric excursions. Conventionally, these cost functions can be derived by solving the Algebraic Riccati Equation (*ARE*). The use of any arbitrary weights leads stable system, but the derived solution will be non-optimal, and such a non-optimal controller may be asking for extra control effort or maybe non-robust. The preceding discussion has driven us to go for optimal *LQR* design for the robust control of *ES*. Various controllers have already been introduced in Section: 4.1 and its relative merits and demerits.

Optimization carried out using heuristic or meta-heuristic methods needs much effort in terms of its exact modeling, training of the model, and framing up the constraints and prove to be worth these efforts where the model is of larger order. Ours is a system where the order of the system never exceeds the 5<sup>th</sup> order, and hence numerical optimization techniques prove more efficient and accurate.

The considered model (2.7) of the *ES* in Chapter:2, is a multiple-input-single-output (MISO) system, wherein the variable grid voltage ( $v_g$ ) is acting as a second (disturbance) input. The disturbance in  $v_g$  has not been taken into account in the modeling of *ES* and its *PI* controller's design, in almost all the prior publications on *ES* (to reduce the complexity in controller design, but with compromised robustness). State-feedback control of *ES*, using the algebraic method of convex optimization for deriving optimally weighted cost functions of *LQR* with an integrator (*LQI*), has been proposed in this chapter by solving Linear Matrix Inequalities (*LMIs*) [73].

## 6.3 Model intricate of the System of Electric Spring

System of *ES* (Fig: 2.14) comprises of a load, bifurcated into critical and non-critical one, and a *VSC* (acting as an *ES*) connected in series with the non-critical load, which further has been connected to the distribution grid through a connecting cable (exhibited

by impedance) and this combination is collectively responsible for maintaining the voltage across the critical load, with its parametric values represented in Table. 2.1. This model, as presented in Sec:2.4.2 of Chapter:2, has numerous uncertainties (mentioned in Sec:2.4.1 of Chapter:2).

Some six such polytopes, due to considered variation in the critical load only i.e.,  $R_{c1}, R_{c2}, R_{c1-L}, R_{c2-L}, R_{c1-C}, R_{c2-C}$ , keeping  $L_g = 0.5 + j0.0942 \Omega$  and  $R_{nc} = 2.2 \Omega$  fixed, could be derived correspondingly as:

$$\begin{aligned}
A_1 &= \begin{bmatrix} -0.1894e5 & -1.6667e5 & 1.2500e5 \\ 500 & 0 & 0 \\ -2459 & 0 & -7049 \end{bmatrix}, A_2 = \begin{bmatrix} -3193 & -1.667e5 & 1.596e5 \\ 500 & 0 & 0 \\ -3193 & 0 & -8691 \end{bmatrix}, \\
A_3 &= \begin{bmatrix} -479 & 54.44 & 0 & 119.8 \\ -1.667e5 & 0 & -1.667e5 & 1.667e5 \\ 0 & 500 & 0 & 0 \\ 7333 & -3333 & 0 & -9000 \end{bmatrix}, A_4 = \begin{bmatrix} -2842 & 54.44 & 0 & 119.8 \\ -1.667e5 & 0 & -1.667e5 & 1.667e5 \\ 0 & 500 & 0 & 0 \\ 7333 & -3333 & 0 & -9000 \end{bmatrix}, \\
A_5 &= \begin{bmatrix} -206.2 & 206.2 & 0 & 453.7 \\ 1.894e4 & -1.894e4 & -1.667e5 & 1.25e5 \\ 0 & 500 & 0 & 0 \\ -833.3 - 2500 & 0 & -7167 & \end{bmatrix}, \\
A_6 &= \begin{bmatrix} -34.77 & 34.77 & 0 & 76.49 \\ 3193 & -3193 & -1.667e5 & 1.596e5 \\ 0 & 500 & 0 & 0 \\ -140.5 & -3193 & 0 & -8691 \end{bmatrix}, \\
B_1 = B_2 = B_3 = B_4 = B_5 = B_6 &= \begin{bmatrix} 0 & 0 \\ 500 & 0 \\ 0 & 3279 \end{bmatrix}, \\
C_1 &= [0.75 \ 0 \ 1.65], C_2 = [0.9579 \ 0 \ 2.107], C_3 = C_4 = [-2.2 \ 1 \ 0 \ 2.2], \\
C_5 &= [0.25 \ 0.75 \ 0 \ 1.65], C_6 = [0.04215 \ 0.9579 \ 0 \ 2.107]
\end{aligned} \tag{6.1}$$

Incorporating all the parametric changes (mentioned in Sec:2.4.1 and using the parameters given in Table:2.1) and deriving the model of the system, makes it a complex

system to be analyzed, for the reason that it turns out to be a polytopic model [68] with  $2^6$  vertices (a version of the polytopic model with limited uncertainties having six vertices, has been presented in (6.1)), and the solution of the same could be figured out iteratively using Linear Programming approach [69] which is cumbersome and time causing. This could be made simpler by transforming such polytopic model into a monotopic model, using certain feasible assumptions, and deriving the controller through Semidefinite Programming (using *LMIs* [73][68]) approach using the concept of modern, robust control. The same is presented in the upcoming sections.

The polytopic model (6.1) has been transformed into a monotopic model, by considering the following assumptions:

- The worst-case critical load of the model with the smallest possible order of the system is considered to reduce the controller design effort.
- Highest possible non-critical load is to be considered, to present the worst-case scenario.
- Moderate grid impedance  $Z_g$  is to be considered.
- Best possible DC-bus voltage is to be considered to reduce the effort of the controller.

Considering all these assumptions and taking into account the parameters prescribed in the Table:6.1, for deriving the model of the system which could further be used for the controller design.

Table 6.1: Parameters of the Considered Model

Parameters	Nomenclature	
Dc Bus Voltage	$V_{dc}$	750V
Filter Inductance	$L_f$	2mH
Filter Capacitance	$C_f$	6 $\mu$ F
Impedance of the Cable	$Z_g$	$0.5 + j0.095\Omega$
Grid Voltage	$v_g$	276V
Critical Load	$R_c$	6.6 $\Omega$
Non-Critical Load	$R_{nc}$	2.2 $\Omega$

The model so derived is represented by  $A_1, B_1, C_1$  (one of the monotope of Eqiaton: 6.1). This model has been considered for the controller design, and from this point onward, it is considered the system's model.

### 6.3.1 State Feedback Control of Electric Spring

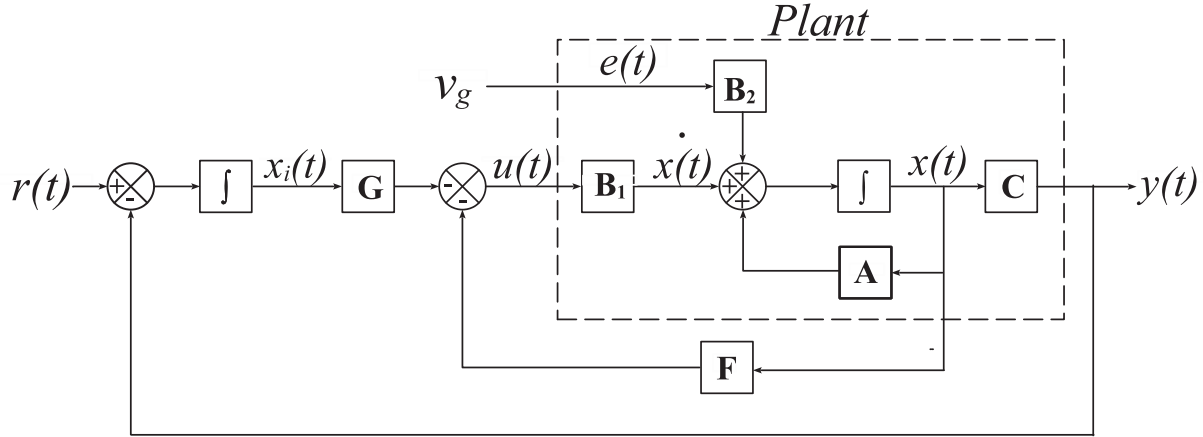


Figure 6.1: Schema of State Feedback controlled *ES*, using *LQI* controller.

State feedback control (*SFC*), if used alone for the control of system of *ES* (inner loop shown in the rectangle), leads to non-zero steady-state error. To achieve zero steady-state error, an integrator has been proposed. The system possessing a *SFC* controller, being incorporated with an integrator, can be seen in Figure. 6.1. The introduction of an integrator adds an additional state ( $x_i$ ), and the same can be represented as,

$$x_i = \int (v_{ref}(\tau) - v_{cr}(\tau) d\tau) \quad (6.2)$$

$$u(t) = -K \cdot x_o(t) = -(F \cdot x(t) + G \cdot x_i(t)), \text{ is the control law governing } SFC, \text{ with} \\ K = [F \ G], \text{ is } SFC \text{ matrix} \quad (6.3)$$

where,

$$x_o(t) = [x(t) \ x_i(t)]^T, \text{ augmented state matrix}$$

$F$  and  $G$ , are Gains of *LQR* and Integrator, respectively

$K$ , gain matrix of *LQI* Controller,

$$r(t) = v_{ref(max)} \cdot \phi, \text{ reference voltage with } (v_{ref(max)} = 230 \times \sqrt{2} \text{ V}) \text{ and}$$

$$\phi = \sin(\omega t + \delta), \text{ signal available from } E\text{-}PLL.$$

Using  $A_1, B_1$  and  $C_1$  of (6.1) and considering (6.2), the resulting augmented state-space model turns out as,

$$\begin{aligned} \begin{bmatrix} \dot{x}(t) \\ \dot{x}_i(t) \end{bmatrix} &= \begin{bmatrix} A & 0 \\ -C & 0 \end{bmatrix} \begin{bmatrix} x(t) \\ x_i(t) \end{bmatrix} + \begin{bmatrix} B \\ 0 \end{bmatrix} U(t) + \begin{bmatrix} 0 \\ I \end{bmatrix} r(t), \\ y_o &= \begin{bmatrix} C & 0 \end{bmatrix} \begin{bmatrix} x(t) \\ x_i(t) \end{bmatrix} \\ \dot{x}_o(t) &= \bar{A}.x_o(t) + \bar{B}.U'_o(t) \\ y_o &= \bar{C}.x_o(t) \end{aligned} \quad (6.4)$$

Where, subscript "o" represents augmented system model,  $I$ - the identity matrix and  $U'_o(t) = [U(t) \ r(t)]^T$ , and the updated A,B,C parameters of the augmented model are,

$$\begin{aligned} \bar{A} &= \begin{bmatrix} -1.89e4 & -1.67e5 & 1.25e5 & 0 \\ 500 & 0 & 0 & 0 \\ -2459 & 0 & -7049 & 0 \\ -0.75 & 0 & -1.65 & 0 \end{bmatrix}; \bar{B} = \begin{bmatrix} 0 & 0 & 0 \\ 500 & 0 & 0 \\ 0 & 3279 & 0 \\ 0 & 0 & 1 \end{bmatrix}; \\ \bar{C} &= \begin{bmatrix} 0.75 & 0 & 1.65 & 0 \end{bmatrix} \end{aligned} \quad (6.5)$$

## 6.4 Design of Optimal Linear Quadratic Regulator for State-Feedback Control

This work resorts to the state feedback controller (static one) design (assuming that all the states are measurable) for stability, regulation, and robustness to control the *ES* for the ultimate desired performance specifications. The augmented system's model (6.5) has failed to satisfy the norm of controllability, which has been negotiated by using the fragmented controller's gain ( $K$ ) into two parts ( $F$  and  $G$ ), for the controller design. Design of gain pertaining to state feedback ( $F$ ) has been carried out through optimization of *LQR*, using  $A_1, B_1$  and  $C_1$  of (6.1), and another part i.e., integrator ( $G$ ) using pole placement method.

For a controllable MIMO system, there happens to be non-unique controller gain matrix  $K$  for which control law is governed by,

$$u(t) = -F.x(t) \quad (6.6)$$

Where,  $F^{m \times n}$ , is the state feedback gain matrix.

Optimization transforms the solution of  $F$ , from non-unique to a unique solution such that the desired pre-set value of  $v_{cr}$  is achieved within the shortest possible time that too with the slightest control effort, in the presence of transients and load variation. The cyclic approach [122] has been considered for simplifying the system's model that is to be used for the *LQR* design.

### 6.4.1 Cyclic Design

The cyclic design transforms a multi-input system into a single-input type by creating a new input, which happens to be the linear combination of multiple inputs of the system,  $\{A, B, C, D\}$ . Cyclicity of a matrix  $A$  can be investigated by the condition of association of unique/distinct eigenvalue associated with each Jordan block of  $A$ . Steps for carrying out the cyclic design are explained as follows:

- Check for the controllability of system having  $n$ -state and  $p$ -input pair  $\{A, B\}$ , using rank of controllability matrix  $C_o (= [B \quad AB \quad A^2B \quad \dots \quad A^{n-1}B])$ , which must be equal to rank of the system.
- if  $A$  is cyclic, then for almost any  $p \times 1$  random vector  $v$ , the single-input pair  $\{A, B.v\}$  is controllable.  $v$  should be as small as possible to restrict the control cost to a smallest possible value.
- Check for the controllability of the modified pair  $\{A, B.v\}$ , if not so, repeat the same by changing  $v$ .
- The modified system  $\{A, B.v, C, D\}$  with the modified input is given by  
 $u(t) = v.u'(t) = -v.k.x(t)$  and  $F = -v.k$

These steps have been followed in redefining the model, to get it converted into a SISO system, to be used in *LQR* design.

Considererig the random value  $v = [0.6991 \ 0.8909]^T$ , and applying the above mentioned steps of cyclic transformation, the modified SISO model has been derived as:

$$\begin{aligned}
 A &= \begin{bmatrix} -1.894e4 & -1.042e4 & 1.562e4 \\ 8000 & -1.183 & -0.3036 \\ -1.967e4 & -3.263 & -7051 \end{bmatrix}, B = \begin{bmatrix} 0 \\ -27.84 \\ 71.63 \end{bmatrix}, \\
 C &= \begin{bmatrix} 192 & 0 & 52.8 \end{bmatrix}, D = 0
 \end{aligned} \tag{6.7}$$

### 6.4.2 Optimal Linear Quadratic Regulator

Optimal *LQR* controller, for the given state feedback  $u$  (6.6), can be designed by minimizing the cost function  $J$  (by penalizing the state and input behavior simultaneously), which can be represented as,

$$J_{min} = \int_0^{\infty} (x^T Q x + u^T R u) dt \tag{6.8}$$

Where,

$x^T Q x$  is state cost, and  $u^T R u$  is the control cost, with corresponding weightage/penalties represented by  $Q^{n \times n}$  and  $R^{m \times m}$ , for a given stabilizable pair  $(A^{n \times n}, B^{n \times m})$  and detectable pair  $(Q, A)$ .

Solution of this optimization problem can be determined by evaluating  $P$  for,

$$A^T P + P A - P B R^{-1} B^T P + Q < 0 \tag{6.9}$$

Here,

$P(= P^T) > 0$ , is Lyapunov variable.  $Q(= Q^T) > 0$  and  $R > 0$  are the inequalities, that justifies (6.9).

Equation (6.9) is called the Continuous-time Algebraic Riccati equation (in the form of a strict inequality). Any arbitrary value of  $Q$  and  $R$  does not guarantee the optimal controller gain matrix  $F$ . The inequality (6.9) could be implemented in the form of Linear Matrix Inequalities (*LMIs*) for finding out the optimal value of  $F$ . The *LMIs* have been detailed in the following subsection.

### 6.4.3 LQR Design using Linear Matrix Inequalities

*LMIs* are matrix inequalities, linear or affine, for a given set of matrix variables. They are essentially meant to be used with convex constraints. An *LMI*, in the canonical form

is presented as,

$$L(x) = L_0 + \sum_{i=1}^m L_i x_i > 0 \quad (6.10)$$

Where,

$L_0 \dots L_m$  are symmetrical matrices of the form  $L_i = L_i^T$ , and  $x = (x_1 \dots x_m)$  represents the vector of decision variables.  $L(x)$  is positive definite and is an affine function of  $x$ . *LMI*s presentation in this form is inefficient from the storage viewpoint and is detrimental to the *LMI* solver, and hence it is presented in the structured form e.g., Lyapunov inequality (6.11).

Lyapunov Inequality, whose satisfactory fulfillment signifies asymptotic stability of a relaxed system ( $\dot{x} = Ax$ ), is a *LMI* and is represented as,

$$A^T P + PA < 0 \quad \text{for } P > 0, \quad (6.11)$$

Our aim, in a feedback control system with  $u = -Fx$  (having  $F = R^{-1}B^T P$ ), is to determine  $F \in \mathfrak{R}^{m \times n}$  such that all the eigenvalues  $A - BF \in \mathfrak{R}^{n \times n}$ , lies in the left half of the  $s$ -plane. Inequality (6.11) in closed loop can be represented as,

$$\begin{aligned} (A - BF)^T P + P(A - BF) &< 0 \\ P^{-1}[A^T P - F^T B^T P + PA - PBF]P^{-1} &< 0 \\ P^{-1}A^T - P^{-1}F^T B^T + AP^{-1} - BFP^{-1} &< 0 \end{aligned} \quad (6.12)$$

The inequality (6.12) is non-linear in nature and can be linearized, by the method of change of variables as,  $Q = P^{-1}$ ;  $\forall Q > 0$  and further  $Y = FQ$ ;  $\forall Y > 0$ . Using these newly introduced variables, (6.12) can be transformed into,

$$QA^T + AQ - Y^T B^T - BY < 0 \quad (6.13)$$

Solving (6.13) for  $Q$  and  $Y$  using any of the iterative approach of Linear Programming, and back substituting the values of  $Q$  and  $Y$ , yields  $P$  and hence  $F$ . Change of variable and back substitution is computationally involving and may not give ample robustness to the controller [123], against parametric excursions. These shortfalls of Eigen Analysis based solution of Lyapunov inequality (6.11) can be negotiated by using Riccati inequality (6.9). Further, (6.11) is a special case of (6.9), with  $B = 0$ . Solving (6.9) for  $P$  ensures asymptotic stability of the closed-loop system through  $F$ , and assures optimality of  $F$  for the reason that (6.9) could be derived from (6.8).

Inequality (6.9) is non-linear in nature and hence it has been converted into *LMI*, using Schur complement Lemma as,

$$\begin{bmatrix} A^T P + PA + Q & PB \\ B^T P & -R \end{bmatrix} < 0 \quad (6.14)$$

Implementing inequalities ( $Q > 0$ ,  $P > 0$ ,  $R > 0$  and (6.14)) in *Robust Control Toolbox* of *Matlab* as *LMIs*, yield  $P$  and  $R$  as,

$$P = \begin{bmatrix} 0.0017 & 0.0000 & -0.0001 \\ 0.0000 & 0.0017 & 0.0000 \\ -0.0001 & 0.0000 & 0.0242 \end{bmatrix},$$

$$R = 15.9047$$

Optimal  $F$  has been found, by substituting the optimally derived values of  $P$  and  $R$  into control law (6.5), where  $F$ ,

$$F = R^{-1} B^T P = [-0.0105 \quad 0.0095 \quad -0.0180] \quad (6.15)$$

and using two distinct values of  $G$  as  $K_{i1} = 25e3$  and  $K_{i2} = 2.5e3$ , yields state feedback gain matrix  $K$  as,

$$K = [F \quad G] = [K_{cf} \quad K_{Lf} \quad K_{Lg} \quad K_i] \quad (6.16)$$

$$= [-0.0105 \quad 0.0095 \quad -0.0180 \quad 25e3] \quad (6.17)$$

$$= [-0.0105 \quad 0.0095 \quad -0.0180 \quad 2.5e3] \quad (6.18)$$

Values of  $F$  and  $G$  have been implemented into the control scheme as depicted in Figure. 6.1, and executed through the controller block shown in Figure. 6.2.

## 6.5 Experimental Arrangement for Testing the Performance of Electric Spring

A test-bench, as presented in Fig: 2.14 of Chapter:2, has been used to test the anticipated performance of *ES* under various load variations and voltage excursions in  $v_g$  (mimicking a practical situation prevailing in the distribution grid). Designed *LQI* controller (6.16) has been tried on the test-bench through the control block presented in Fig: 6.2. A

feed-forward compensation has been added, in *LQI* control [71], to avert the impact of transients and achieve smooth transition at the advent of load change. Grid voltage  $v_g$  has been varied along with the load (varied with load variants) at the time instances mentioned in Table. 6.2.

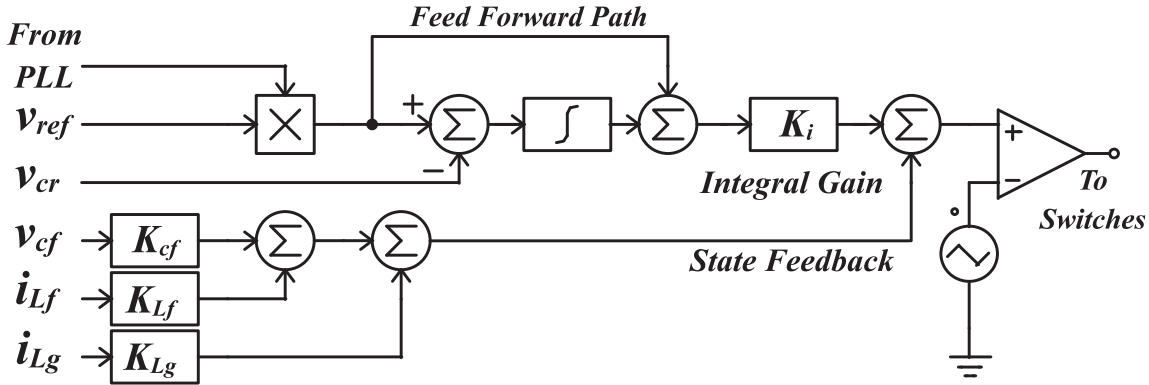


Figure 6.2: The control block of *ES*, with *LQI* control.

## 6.6 Analysis and Evaluation of Results

The performance of the system (modeled as  $A_1, B_1, C_1$  of (6.1), being controlled by state-feedback control (using *LQI* controller), has been evaluated through the step response and frequency response analysis. These performance benchmarks have been justified and validated through the performance of the test-bench (Figure.2.14), by executing its control through the said controller depicted in Figure.6.2.

### 6.6.1 Frequency Response Analysis

Figure. 6.3 shows the bode plot of the system's model considered under three different configurations viz. loop gain of the system, (a) in open loop, (b) with the *LQR* controller (6.15), and (c) with *LQI* controller (6.16). The plot of loop gain with state feedback gain (6.17) using  $K_{i1} = 25 \times 10^3$  yields a *P.M.* of  $85.7682^\circ$  and a *G.M.* of  $122.6678db$ , which is sufficient to be implemented in the test bench (Figure.2.14) possessing limited parametric uncertainties (considering the variation in Load and grid voltage only), but it proves non-sufficient in terms of robustness in the case where all the uncertainties (also

including the variation in  $Z_g$  and  $V_{dc}$ ) is required to be considered and to be implemented in test bench (subject matter of the Chapter:7). The plot also shows the loop gain of the system with state feedback gain (6.18), using  $K_{i2} = 2.5 \times 10^3$ , exhibiting a slightly higher  $P.M.$  of  $89.5585^\circ$  and a much larger  $G.M.$  of  $122.6678 \times 10^3 db$  (when being compared with that achieved through  $K_{i1}$ ), showing a greater bandwidth and hence robustness. The cost of additional gain and bandwidth is to be paid in terms of sluggish response, and the same can be depicted from the step response of the system (Fig:6.4). Looking at the

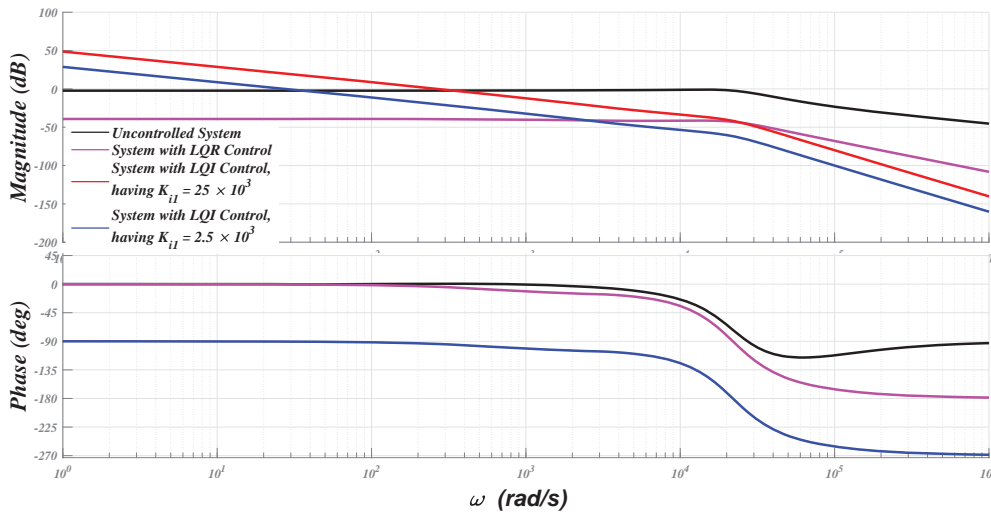


Figure 6.3: Bode plot of the system under various system conditions.

Bode plots, it is evident that the set aside design goals (of larger  $G.M.$  and  $P.M.$ ) have been achieved through the designed controller.

### 6.6.2 Step Response Analysis

Figure. 6.4 shows the step response of the system, with three distinct situations, named as (a) system under the influence of disturbance input, i.e., when  $v_g$  is acting alone in the system (in the absence of  $ES$ ), (b) system with  $LQR$  control and (c) system with  $LQI$  control. Furthermore, based on the demanded robustness and speed, two distinct scenarios have been presented through the step response analysis, by varying the Integral gain  $K_i$ , i.e.,  $G$  of the  $LQI$  controller, keeping the gain associated with the state feedback, i.e.,  $F$  constant. It shows nice and stable output, with both the  $SFC$  gains, without any overshoot. As far as the performance of the step response is concerned, it has been swiftly

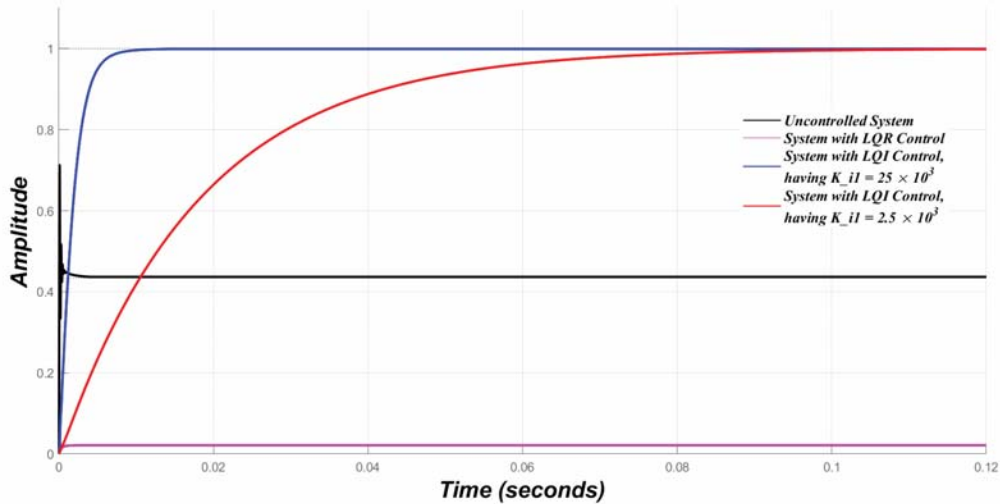


Figure 6.4: Step response of uncontrolled system, *LQR* controlled system and *LQI* controlled system.

achieving the unity gain with  $K_i = 25000$  ( $t_s < 5ms$ ) as that compared to  $K_i = 2500$  ( $t_s = 60ms$ ). The faster response is being compromised with inferior bandwidth, and the same is evident from the frequency response plot of Fig:6.3.

Looking at the frequency response plot and the step response, it has been decided to implement the state feedback gain (6.17) using  $K_i = 25000$  for the implementation with simulation test-bench (Fig: 2.14), for limited parametric excursions, and the corresponding results have been presented in the following section.

### 6.6.3 Performance Analysis of Test-Bench

The system is shown in Figure. 2.14, using the parameters exhibited in TABLE. 6.1, has been simulated to validate the results of the Bode plot and Step response. The critical load has been varied by switching it in a specific configuration, by keeping the non-critical load fixed at  $2.2 \Omega$ . The same has been mentioned in TABLE. 6.2 with the corresponding time instances. The scenario of the absence of *ES* has not been presented here as it has already been presented in Table:2.3. The results associated with the variation of the parameters have been assimilated here, in the form of Figures (Fig:6.5 through Fig:6.12), and tabulated in the abstract form in Table: TABLE. 6.2. Change in the load and the perturbations in  $v_g$  can also be witnessed from the presented figures, mimicking the

intermittency in the grid voltage inflicted by RES. Reference Phase angle  $\delta$  of  $v_{ref}(t)$  (6.2) has been extracted from  $v_g$ , through Enhanced Phase Locked Loop (*E-PLL*) structure designed and presented in Sec:3.6.3. Fig:6.5 and Fig:6.12 presents the absolute spectrum of the perturbing parameters. Fig:6.6 through Fig:6.11 shows the magnified view of the the Fig:6.5, depicting perturbations in the parameters in the presence of a typical load variant, in the presence of changing grid voltage.

Table 6.2: Variation of Parameters, with Optimal *LQI* Control, with Respect to Time

<i>Time(s)</i>	<i>Load<math>\Omega</math></i>	$V_g(V)$	$V_{nc}(V)$	$V_{es}(V)$	$I_g(A)$	$I_{nc}(A)$	$I_{cr}(A)$	$I_{inv}(A)$	<i>Power(W)</i>	$V_{cr}(V)$	%Reg. $V_{cr}$	% Imp. In Reg.
0.00-0.33	6.6 + j5.78	183.85	250.48	475.25	90.59	113.86	26.23	113.81	20147.90	230.00	0.00	37.43
0.33-0.66	6.6 + j5.78	229.81	54.52	276.69	3.39	24.78	26.21	24.69	159.01	229.95	-0.02	21.76
0.66-1.00	6.6 + j5.78	275.77	149.78	81.89	90.60	68.08	26.21	68.21	-20089.00	229.89	-0.05	6.10
1.00-1.33	50 + j5.78	183.85	210.03	438.62	90.90	95.47	4.57	95.50	20248.40	230.20	0.09	35.53
1.33-1.66	50 + j5.78	229.81	14.46	242.85	3.91	6.57	4.57	7.26	266.82	230.12	0.05	19.35
1.66-2.00	50 + j5.78	275.77	188.60	70.58	90.24	85.73	4.57	85.90	-19992.20	230.05	0.02	3.18
2.00-2.33	6.6 - j5.78	183.85	241.59	471.99	91.43	109.81	26.27	109.90	20381.30	230.41	0.18	37.05
2.33-2.66	6.6 - j5.78	229.81	65.38	281.12	3.73	29.72	26.26	30.15	365.20	230.36	0.16	21.24
2.66-3.00	6.6 - j5.78	275.77	172.10	122.08	89.71	78.23	26.26	78.51	-19916.80	230.29	0.13	5.43
3.00-3.33	50 - j5.78	183.85	209.70	438.48	90.92	95.32	4.57	95.35	20254.70	230.17	0.07	35.50
3.33-3.66	50 - j5.78	229.81	15.80	243.02	3.95	7.18	4.57	7.87	274.51	230.13	0.06	19.33
3.66-4.00	50 - j5.78	275.77	189.18	72.29	90.21	85.99	4.57	86.17	-19986.60	230.05	0.02	3.16
4.00-4.33	6.6 + j0.00	183.85	276.33	505.52	91.12	125.60	34.89	125.60	20282.50	230.25	0.11	38.82
4.33-4.66	6.6 + j0.00	229.81	79.60	309.59	3.15	36.18	34.88	36.31	263.20	230.18	0.08	23.48
4.66-5.00	6.6 + j0.00	275.77	125.44	125.77	90.05	57.02	34.87	57.30	-20009.30	230.13	0.06	8.13
5.00-5.33	50 + j0.00	183.85	210.00	438.69	90.92	95.46	4.60	95.49	20252.70	230.17	0.07	35.51
5.33-5.66	50 + j0.00	229.81	15.21	243.07	3.92	6.91	4.60	7.60	271.69	230.12	0.05	19.35
5.66-6.00	50 + j0.00	275.77	188.75	71.51	90.22	85.80	4.60	85.97	-19989.20	230.05	0.02	3.18

Fig: 6.5 through Fig: 6.12, shows the variation of  $v_g$  (184V to 276V RMS) and the corresponding variation of  $v_{cr}$ , in the absence of *ES* (141V to 223V). This drop in the voltage is due to the impedance of the conductor ( $Z_g$ ), connecting the load to the grid, and variation in the same due to variation in the connecting point (as mentioned in Sec:2.6) is acting as a miscreant and debilitates the stability in the absence of non-robust controller design.

Fig:6.5 through Fig: 6.11 shows the variation of  $v_{cr}$  in the case when it is being controlled by *LQI* controller (229.89V to 230.41V) at the wake of change in the load and changing grid voltage (as presented in Table:6.2), and corresponding % regulation is seen to be varying in the range of "−0.05" to "+0.18" % which refers to a variation of only 0.23%. The results show quite precise and excellent voltage regulating capabilities of the *LQI* controller, further justifying the controller design's efficacy, robustness, and

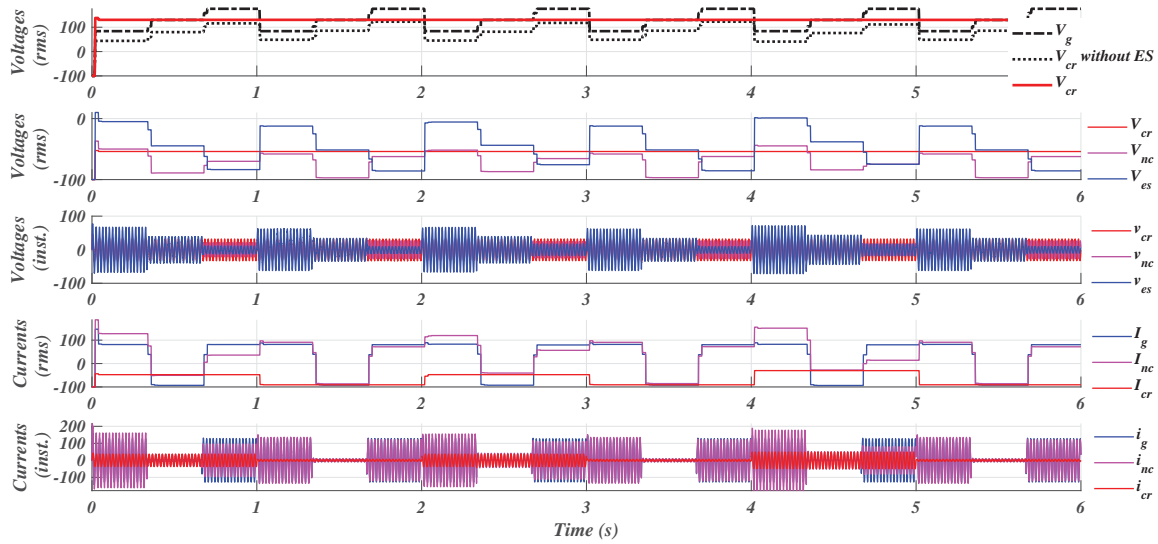


Figure 6.5: Absolute Spectrum of  $LQI$  Control having Step Changes Applied to  $v_g$  and Load.

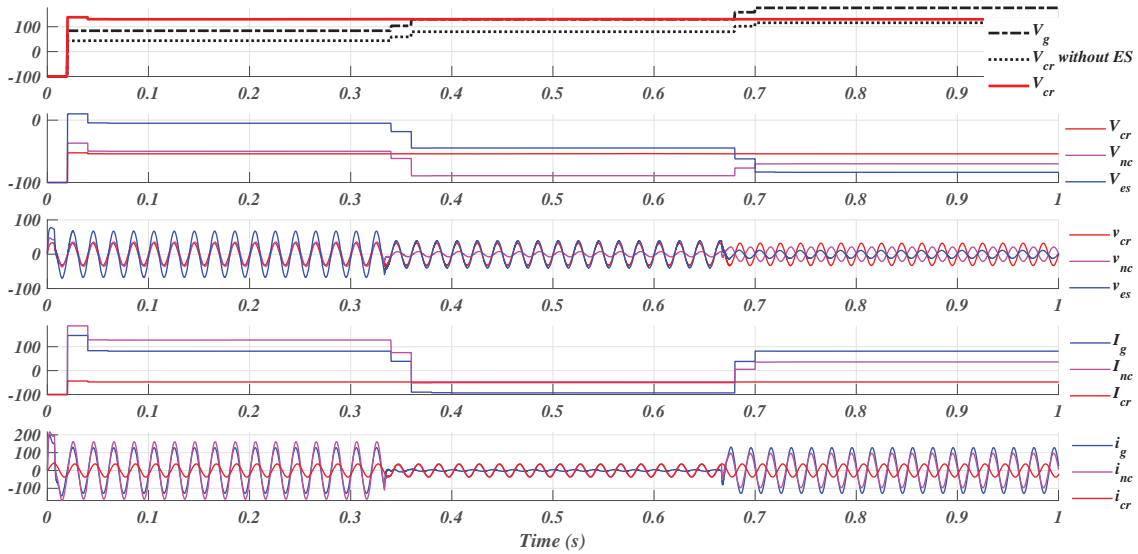


Figure 6.6: Results of  $LQI$  Control having Step Changes in  $v_{cr}$ , for  $R_1$ - $L$  Load.

precision.

Fig:6.5 through Fig: 6.11 also exhibit the variation in  $i_{cr}$  without  $ES$  (2.96A to 32A), and with  $ES$  (4.57A to 34.89A with  $LQI$  control). It also shows the variation in the current of non-critical load ( $i_{nc}$ ), without  $ES$  (6.5A to 102.1A), and with  $ES$  (7.16A to 127.7A with  $LQI$  control). These results also reveal that  $ES$  damps out current alterations due to variation in  $v_g$  (for a specific load type) at the cost of variation in non-critical load

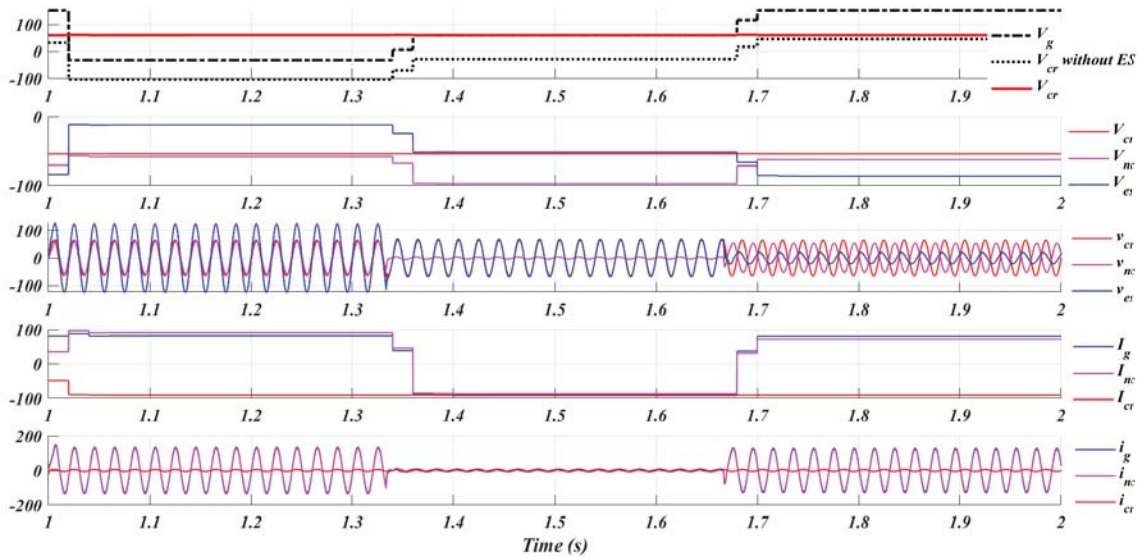


Figure 6.7: Results of  $LQI$  Control having Step Changes in  $v_{cr}$ , for  $R_2$ - $L$  Load.

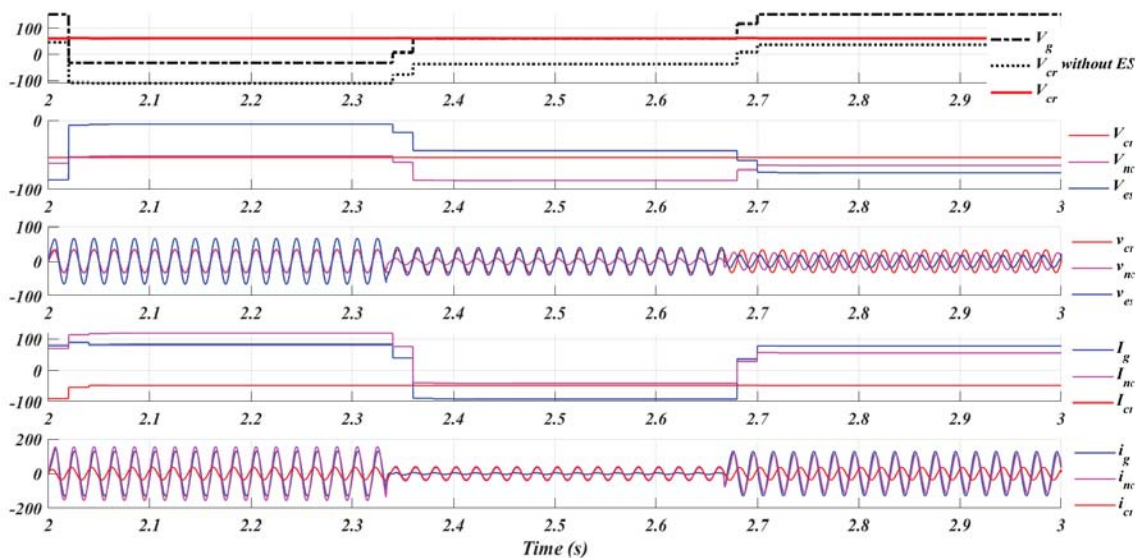


Figure 6.8: Results of  $LQI$  Control having Step Changes in  $v_{cr}$ , for  $R_1$ - $C$  Load.

current. Constant  $i_{cr}$  for a typical load, in the presence of perturbing  $v_g$ , has been an indicator of the efficacy of  $ES$  in terms of its voltage regulating abilities.

Fig: 6.12 exhibit the variation of  $Power$  that is being exchanged between the grid and with  $ES$  ( $-20$  KW to  $20$  KW with  $LQI$  control) which otherwise varies in the range of  $8.6$  KW to  $28$  KW, in the absence of  $ES$ . Here, ”  $+Ve$ ” sign signifies the flow of power from  $ES$  to load, and ”  $-Ve$ ” sign signifies the flow of the same from the grid. The presence of  $ES$  reveals a formidable peak power shaving (of about  $8$  KW).

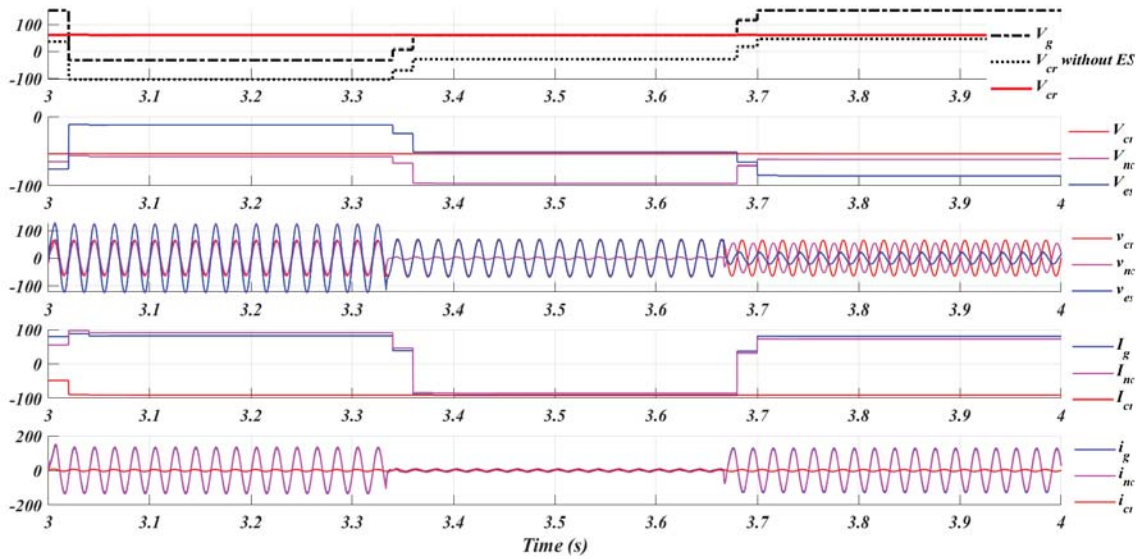


Figure 6.9: Results of  $LQI$  Control having Step Changes in  $v_{cr}$ , for  $R_2$ - $C$  Load.

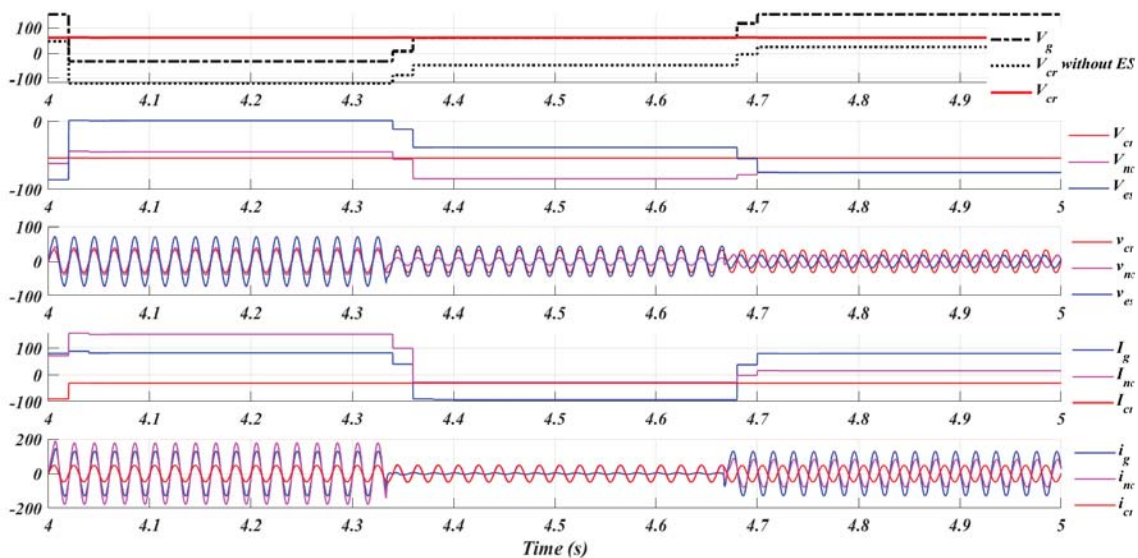


Figure 6.10: Results of  $LQI$  Control having Step Changes in  $v_{cr}$ , for  $R_1$  Load.

Instantaneous variation of  $v_g$ ,  $v_{cr}$ ,  $v_{nc}$ ,  $i_g$ ,  $i_{cr}$ , and  $i_{nc}$  through the graphical results reveal the smooth transition of voltage and current signals, at the wake of perturbing load and grid supply. At the wake of such transitions, voltages and currents settle quick enough (in less than one-half cycle) to validate the claims presented in the step response (Figure. 6.4). Smooth transition and absence of large overshoot, at the transition, proves the worth of feed-forward path (Figure. 6.2).

All the possible and diverse scenarios of load and voltage perturbations (of  $LQI$

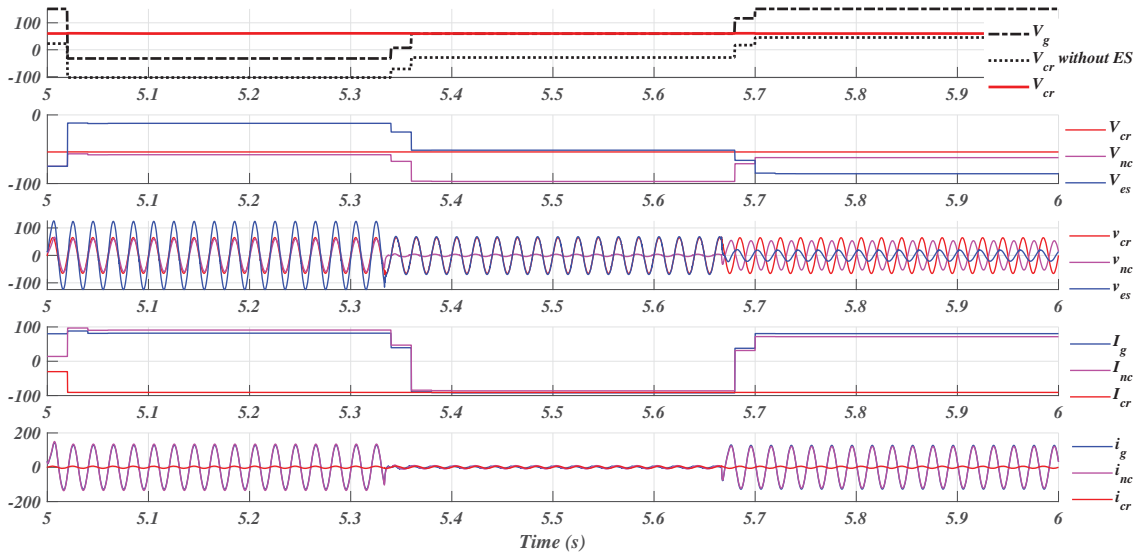


Figure 6.11: Results of  $LQI$  Control having Step Changes in  $v_{cr}$ , for  $R_2$  Load.

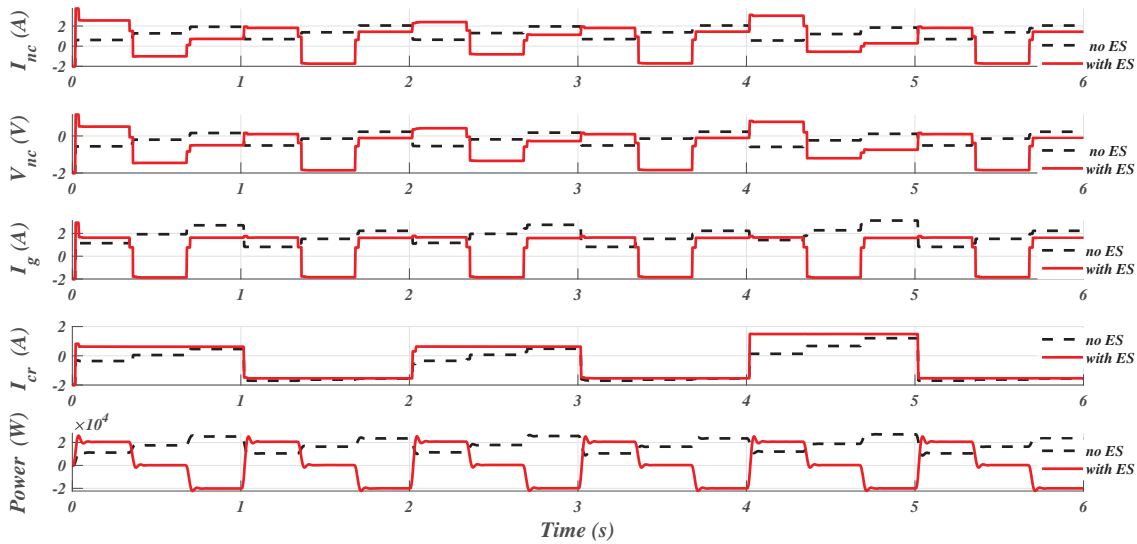


Figure 6.12: Comparison of Results of  $LQI$  Controlled  $ES$  and that with no  $ES$ , under the influence of Step Changes in  $v_g$  and Load.

controlled  $ES$ ) have been presented through phasors in Figure. 6.13, as mentioned in TABLE.6.2. These phasors have been drawn to the scale (1:1), from the data of simulation results using AutoCAD.  $v_g$  has been considered a reference phasor, having its origin (of all the cases) placed on a vertical dotted line. All the cases (associated with a typical load type) reveal the locus of the  $v_{cr}$  falling on the circles with the magnitudes mentioned in TABLE. 6.2 (all these circles touching on the other dotted line, spaced apart at a

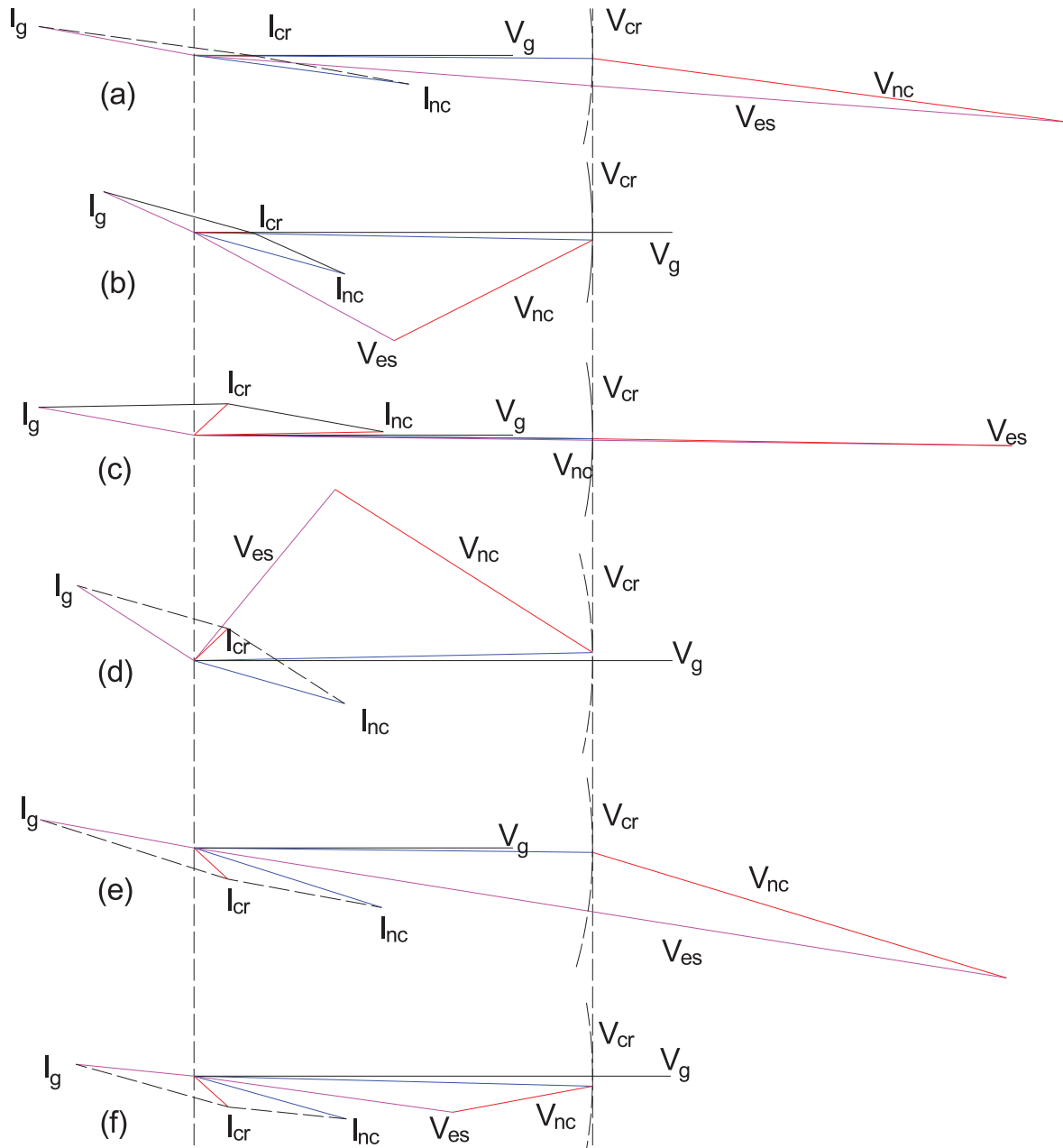


Figure 6.13: Phasors of LQI controlled system, with (a)  $R$  Load when  $v_g < v_{ref}$ , (b)  $R$  Load when  $v_g > v_{ref}$ , (c)  $R-C$  Load when  $v_g < v_{ref}$ , (d)  $R-C$  Load when  $v_g > v_{ref}$ , (e)  $R-L$  Load when  $v_g < v_{ref}$ , and (f)  $R-L$  Load when  $v_g > v_{ref}$ .

distance of  $v_{ref}$  (230V)), indicates excellent voltage regulating capability of  $ES$ . It also shows that a second-generation  $ES$  can support active as well as reactive power (power being delivered when  $v_g < v_{ref}$  and same being absorbed when  $v_g > v_{ref}$ ), so as to track the reference voltage ( $v_{ref}$ ).

## 6.7 CONCLUSION

Custom power device, *ES* provides an opportunity for the non-critical load to act as a part of smart load, managing the voltage regulation across the critical load in a very tight band by manipulating and utilizing voltage across it ( $v_{es}$  and  $v_{nc}$ ), with no extra overhead of communication interface. *ES* reduces the fluctuation in current  $i_{cr}$ , by smartly manipulating  $i_{nc}$ , in the presence of greater excursions in grid voltage and grid impedance, conditions commonly experienced in most of the rural and even some of the urban Indian distribution grid in the presence of *RES*. Design of control system of *ES* having considerably larger bandwidth and small control effort, with shortest possible settling time, is a task having conflicting control requirements, under the wake of large scale and vivid excursions in load and grid conditions. The results reveal the superior performance of the designed state feedback-based optimal *LQI* controller compared to that of a *PI* controller, exhibiting robustness against parametric excursions and good response speed ( $t_s < 10$  ms), and small demand for control energy. The onerous task of negotiating with the conflicting controller requirements has significantly been satisfied, thanks to numerical convex optimization of state feedback controller gain, being carried out through a simple method of *LMIs*. Electric Spring controlled by the proposed *LQI* controller comprehensively ensures the desired constant voltage across the critical load, with peak power shaving and hence commensurating with the concept of demand-side management in real-time.